
Article:
Bačić, Goran, Rankine, Conor D orcid.org/0000-0002-7104-847X, Masuda, Jason D et al. (2 more authors) (2020) Volatile and Thermally Stable Polymeric Tin Trifluoroacetates. Inorganic Chemistry. 996–1005. ISSN 0020-1669

https://doi.org/10.1021/acs.inorgchem.9b01308

Volatile and Thermally Stable Polymeric Tin Trifluoroacetates

Goran Bačić,*† Conor D. Rankine,‡ Jason D. Masuda,¶ Derek A. Wann,‡ and Seán T. Barry†

†*Department of Chemistry, Carleton University, 1125 Colonel By Drive, Ottawa, Ontario, Canada K1S 5B6*
‡*Department of Chemistry, University of York, Heslington, York, United Kingdom YO10 5DD*
¶*Department of Chemistry, Saint Mary's University, 923 Robie Street, Halifax, Nova Scotia, Canada B3H 3C3*

E-mail: gibacic@gmail.com

Abstract

Tin trifluoroacetates are effective vapor phase single-source precursors for F-doped SnO_2, but their structures have been poorly understood for decades. Here we undertook a comprehensive structural analysis of these compounds in both the solid and gas phases through a combined single-crystal X-ray crystallography, gas phase electron diffraction, and density functional theory investigation. Tin(II) bis(trifluoroacetate) (**1**) thermally decomposes into a 1:1 mixture of **1** and ditin(II)-μ-oxy-bis-μ-trifluoroacetate (**2**) during sublimation, which then polymerize into hexatin(II)-di-μ_3-oxy-octakis-μ-trifluoroacetate (**3**) upon solidification. Reversible depolymerization occurred readily upon heating, making **3** a useful vapor phase precursor itself. Tin(IV) tetrakis- (trifluoroacetate) (**5**) was also found to be polymeric in the solid state, but it evaporated as a monomer over 130 °C lower than **3**. This counterintuitive improvement in volatility by polymerization was possibly due to the large entropy change during sublimation, which offers a strategic new design feature for vapor phase deposition precursors.

Introduction

Demand for transparent conductors made entirely of earth-abundant elements like F-doped SnO_2 is rising due to economic and environmental concerns.[1–4] Atomic layer deposition (ALD) and chemical vapor deposition (CVD) are attractive high performance methods for their fabrication, and have become prevalent in industry.[5,6] However, there are currently no ALD processes to deposit F-doped SnO_2, likely because fluorine doping agents are hazardous (e.g., HF)[7,8] or are difficult to use (e.g., metal fluorides, decomposition of fluorinated ligands).[6,9,10] We set out to evaluate fluorinated single-source precursors with the hopes of developing a simple ALD process that can be integrated into real-world device architectures.

Trifluoroacetic acid (HO_2CCF_3) is an inexpensive, non-toxic, and environmentally benign ligand.[11] Tin(II) bis(trifluoroacetate) (**1**) is known to be one of the best precursors for F-doped SnO_2 by CVD:[12–14] highly transparent films with low resistivities were deposited at atmospheric pressure above 200 °C with high growth rates using air as the co-reactant. Compound **1** was only been reported once, and was prepared by condensing blue-black tin(II) oxide with an excess of trifluoroacetic acid and trifluoroacetic anhydride.[15] Additionally, it was only characterized by microanalysis, FTIR and ^{119}Sn Mossbauer spectroscopy; while structural investigations were hindered by polymerization, thermal decomposition, and oxidation.[15,16] Despite their simple composition, tin trifluoroacetates have seen only a handful of structural analyses over the last three decades.[15–18] We wished to gain a fundamental insight into the structure–property relationships of tin trifluoroacetates to better understand their suitability as vapor phase precursors.

Traditionally, oligomers and polymers were presumed to be non-volatile due to their extreme molecular weight,[19] and great lengths were usually taken to ensure that precursors are monomeric by design.[20] While some volatile CVD precursors were coincidentally polymeric,[21] the

features that made some polymers volatile has not been described. Here we prepare and evaluate tin trifluoroacetates as potential vapor phase precursors under realistic conditions. Our results show that polymerization can be exploited to dramatically and counterintuitively improve volatility, possibly by a large change in entropy during evaporation from a polymer to monomers. The high volatility and thermal stability of these simple fluorinated compounds, especially compared to their hydrogenated analogues, make them promising precursors for vapor deposition of F-doped SnO_2.

Results and Discussion

While trying to make tin(II) bis(trifluoroacetate) (**1**) by oxidation of Sn^0 with copper(II) bis(trifluoroacetate) in deoxygenated water (Equation 1),[22] we obtained a colorless powder after prolonged drying under high vacuum. From this crude product we were able to sublime a colorless powder (150 °C, 10 mTorr) without any non-volatile residue, which itself could be sublimed and recovered quantitatively. The crude yield of this synthesis was moderate (ca. 65%) assuming conversion to **1**. However, both mass spectrometry and NMR spectroscopy were not consistent with the formulation of **1**, but rather another unknown species. A combined density functional theory (DFT) and gas phase electron diffraction (GED) approach was used to unambiguously determine the species that evolved during sublimation and by extension infer the composition of the unknown solid. Our initial structural guesses were guided by electron impact mass spectrometry (EIMS, Figure S1, Supporting Information), and we determined that there was an equal mixture of **1** and ditin(II)-μ-oxy-bis-μ-trifluoroacetate (**2**) in the gas phase by the exceptional agreement between our theoretical and GED data (Figure 1, and Figures S3-5, Supporting Information).

$$Sn^0 + Cu(O_2CCF_3)_2 \rightarrow Cu^0 \downarrow + Sn(O_2CCF_3)_2\ (\mathbf{1}) \qquad (1)$$

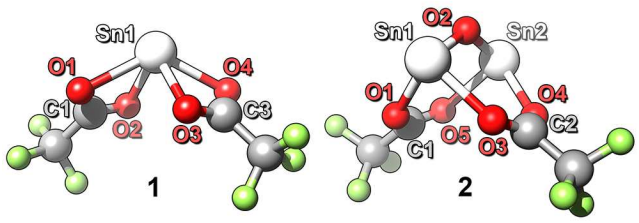

Figure 1. Gas phase products of the thermal depolymerization of **3** determined by GED; tin(II) bis(trifluoroacetate) (**1**, left) and ditin(II)-μ-oxy-bis-μ-trifluoroacetate (**2**, right).

The unknown solid was also isolated during the sublimation of **1** prepared by the previously reported method,[15] which was also confirmed by NMR, EIMS, and GED. A single crystal suitable for X-ray crystallography was grown by slowly cooling a doubly sublimed sample of the unknown solid in toluene. Upon structural determination, we confirmed it was in fact the polymeric hexatin(II) di-μ_3-oxy-octakis-μ-trifluoroacetate (**3**, Figure 2), which had a stoichiometry that equaled a mixture of **1** and **2** (Equation 3). Thermal depolymerization of **3** into **1** and **2** was reversible, and **3** was recovered quantitatively after repeated sublimations. If the material isolated following both synthetic methods before heating under vacuum was in fact **1**, it is likely that **1** decomposes by eliminating trifluoroacetic anhydride during sublimation to form gaseous **1** and **2** (Equation 2), which polymerize into **3** upon solidification (Equation 3). The oxidation of metallic tin was easily scalable, and multigram batches (>25 g) were routinely prepared in good yields. Benign metal waste, mild reaction conditions, and simple workup make it a convenient green synthetic protocol[23] and the most promising route to prepare **3**.

$$3\ Sn(O_2CCF_3)_2\ (s)\ (\mathbf{1}) \rightarrow \mathbf{1} + Sn_2O(O_2CCF_3)_2\ (g)\ (\mathbf{2}) + (CF_3CO)_2O\ (g) \quad (2)$$

$$\mathbf{1} + \mathbf{2} \rightleftarrows \tfrac{1}{2}\ Sn_6O_2(O_2CCF_3)_8\ (s)\ (\mathbf{3}) \quad (3)$$

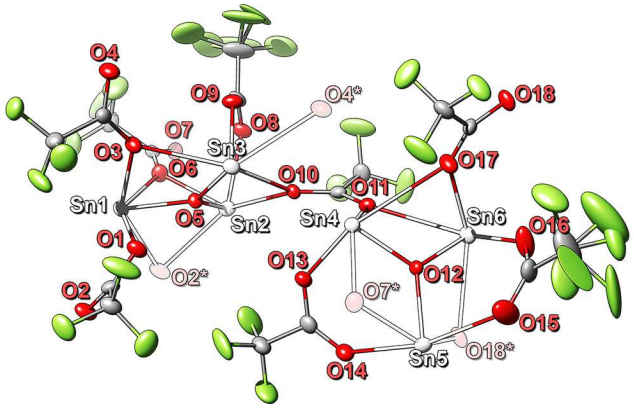

Figure 2. An asymmetric monomer of hexatin(II) di-μ_3-oxy-octakis-μ-trifluoroacetate (**3**). Ellipsoids are set to 50% probability, disordered CF_3 groups are included, and intermolecular contacts are drawn translucent.

In the solid state, asymmetric units of **3** were linked by covalent bonds between Sn5 on one and O18* on another (2.360(3) Å), making each a monomer within an extended polymeric chain (Figure 3). These chains packed in a crystal structure with longer Sn–O_2CCF_3 intra- and intermolecular coordination where the Sn^{II} atoms formed distinct and extremely distorted pseudo-square pyramidal geometries (Figure 4). We could glean no obvious trend from the coordination geometries. The plastic behaviour of **3** in the solid state, its facile thermal depolymerization into **1** and **2**, and its seemingly random Sn–O_2CCF_3 bond lengths suggested the ligands in **3** were labile in the condensed phase. Nevertheless, by comparing the five shortest Sn–O distances in **3**, we were able to group the Sn–O bonds into three types: "weak" above average length bonds, "strong" below average length bonds, and short μ_3-oxy bonds (Figure S9, Supporting Information). These bond definitions ultimately revealed the fate of the structural elements of **3** when evaporating into **1** and **2** (Figure 5).

Each Sn atom in **3** was bound to trigonal planar μ_3-bridging oxygen atoms with similar bond lengths (ca. 2.0 Å with a 0.2 Å deviation of μ_3-O from Sn–Sn–Sn plane). This was reminiscent of the recently prepared "trapped" SnO complex.[24] Natural bond order (NBO) analysis

previously showed the trapped oxygen to have a strongly ionic character with three σ-bonds from lone pairs on the oxygen to empty orbitals on the three Sn atoms. Despite similarities, it is misleading to describe the μ_3-oxygen in **3** as representing a "trapped" SnO species: one of the three Sn–μ_3-O bonds was shorter than the other two (i.e., Sn3 and Sn6), opposite to what was expected for trapped SnO donating to two other Sn atoms. This suggested that two Sn atoms in the Sn_3–μ_3-O group formed Lewis basic covalently bound Sn–O–Sn bridges, and the other accepted σ-electron density as a Lewis acid. Frontier orbital analysis of **1** and **2** supported this description, implying **3** was the polymeric Lewis pair $(\mathbf{1}\leftarrow\mathbf{2})_\infty$ (Figure 5). This was an important distinction since it also predicted that the polymer should break into these Lewis acid/base units upon evaporation, as observed by GED. The orbital energies and distributions in the **1** and **2** fragments supported their roles as acid and base, respectively. Only the basic Sn–O–Sn bridge in **2** and complementary acidic orbitals in **1** had the appropriate symmetry to allow overlap to form Lewis pairs (Figure 6).

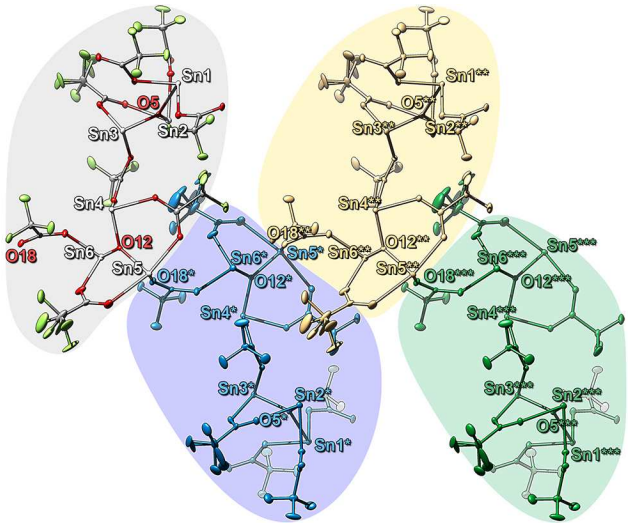

Figure 3. Polymeric chain of $(\mathbf{3})_4$. The first monomer (leftmost, gray highlight) is shown in Figure 1 (colored by element), while the other monomers are uniformly colored and highlighted (blue, yellow, and green from left to right) for clarity. Monomers are covalently bound through Sn5 – O18* bonds.

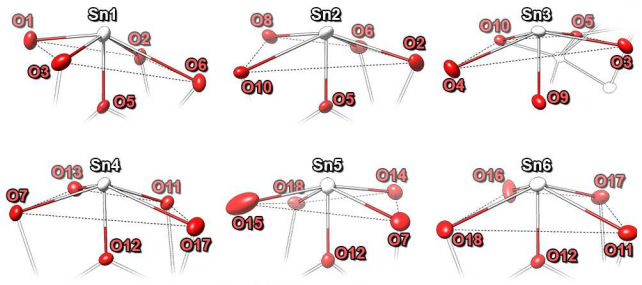

Figure 4. Extremely distorted pseudo-square pyramidal geometry around each Sn atom in **3**. Only the five shortest Sn–O interactions are shown.

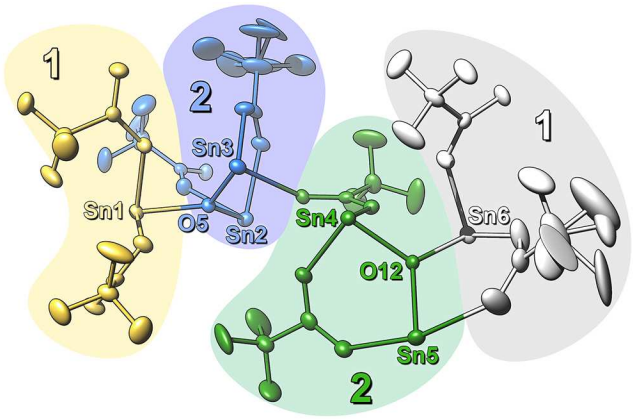

Figure 5. Asymmetric unit of **3** showing the fate upon evaporation of Sn1 and Sn6 as **1** (gold, white; left and right) and Sn[2-3] and Sn[4-5] as **2** (blue, green; middle).

Our difficulty growing crystals of **3** was not surprising. Previous reports of attempts to grow single crystals of **1** produced species like those we isolated. Compound **3** ligated with free trifluoroacetic acid was previously grown by heating **1** in a sealed evacuated tube, where protons from hydroxyl groups on the tube's walls were presumably abstracted by trifluoroacetic anhydride to form the acid ligand.[16] The hydrated cluster compound tetratin(II) monotin(IV) di-μ_3-oxy-octakis-μ-trifluoroacetate (**4**) was previously grown by oxidation in $O(OCCF_3)_2/HO_2CCF_3$;[15] while we found crystals of anhydrous **4** near the seal of a pressure vessel after sublimation of pure **3** (Figure 11), presumably formed by oxidation with air that diffused through a degraded O-ring seal. Both of these previously reported compounds share structural motifs with **3**, highlighting the rich coordination chemistry in this tin-oxy-trifluoroacetate system.

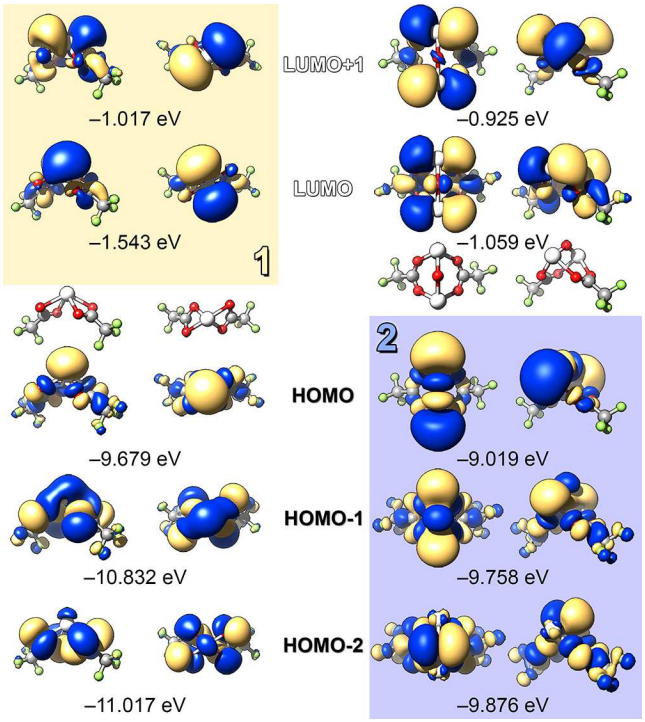

Figure 6. Frontier orbitals of **1** (left) and **2** (right), calculated with the SOGGA11-X functional and DKH-TZP basis set, viewed from the top (inside) and sides (outside). Lewis acidic and basic orbitals with the correct orbital symmetry overlap are highlighted in gold and blue, respectively.

Tin(IV) tetrakis(trifluoroacetate) (**5**) was also polymeric in the solid state, and yet was surprisingly volatile. A single crystal suitable for X-ray crystallography was grown by sublimation under nitrogen in a gently heated sealed tube (ca. 50 °C). The structure of **5** consisted of symmetrical, linear, non-interacting polymeric chains of octahedral Sn^{IV} with four equatorial μ-bridging and two monodentate axial ligands (Figure 7). Unlike **3**, compound **5** was very sensitive to air and moisture, and its preparation and handling were more difficult. But its combination of high volatility and reactivity, along with a lack of Sn–C bonds gives **5** the potential to be a near-room temperature precursor for SnO_2 that may bypass current issues of low growth rate and high carbon contamination from other precursors.[25,26] GED analysis showed that **5** evolves the expected monomer **6** with pseudo-dodecahedral coordination of four η_2-trifluoroacetates upon evaporation

(Figure 8). As with compound **3**, the bulk composition of **5** was supported by the high quality of our refined GED data.

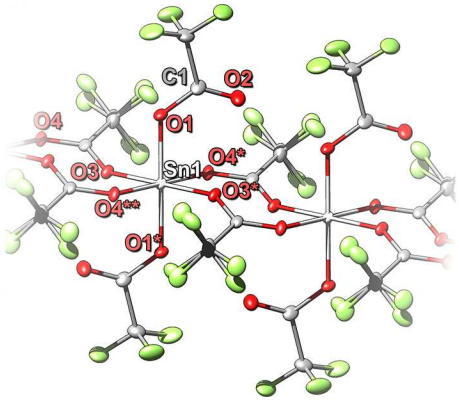

Figure 7. Solid state structure of polymeric **5**. Disordered CF_3 groups are shown, and ellipsoids are displayed at 50% probability.

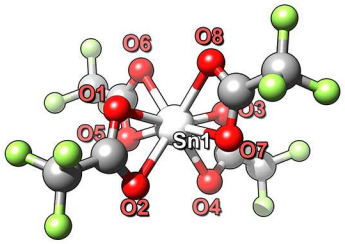

Figure 8. Gas phase structure of **6**.

The solid state structures of **3** and **5** showed differences to their hydrogenated cousins tin(II) diacetate (**7**) and tin(IV) tetraacetate (**8**). Both **3** and **7** are linear polymers via "strong" Sn–O bonds (vide supra), where each Sn atom is tetracoordinate with Sn–OAc bonds in the range 2.17-2.37 Å.[27] However, **3** displays interchain coordination via bridging trifluoroacetate ligands while **7** forms tetrameric columns of $(\mathbf{7})_n$ chains with their stereochemically active lone pairs oriented inward and acetate ligands outward. This organization was explained as a steric effect, but the possibility of CH_3–O interactions could not be ruled out.[27] Compounds **1** and **7** are isostructural in the gas phase with C_2 symmetry, showing very similar Sn–O bond lengths [2.186(22) and 2.395(25) vs. 2.192(8) and 2.337(12), respectively].[28] This is different from the

gas-phase structure of **2**, and there is no precedent in the literature of compounds with an unligated Sn^{II}–O–Sn^{II} bridge, making **2** the first structurally characterized example. Comparison of **6**, the gas phase monomer of **5**, with the solid state structure of **8** show both are pseudo-dodecahedral with four bidentate ligands and similar Sn–O bond lengths in the range 2.13-2.29 Å.[29]

Thermogravimetric analysis (TGA) of **3** and **5** showed their excellent thermal stability and volatility compared to **7** and **8** (Figures 9 and 10). Both **3** and **5** had single step volatilization with no decomposition, which was ideal behaviour for potential ALD precursors. Decomposition during TGA can be evaluated simply by increasing the initial mass loading, in what is called a "thermal stress" test.[20] Simply, a higher loading of analyte requires more time to evaporate, so a higher mass of analyte is exposed to higher temperatures for longer time. Thus, higher temperature decomposition events may occur and be observed during an experiment as an increase in non-volatile residual mass. This stress test can be used to qualitatively evaluate the onset of decomposition and overall stability of a potential precursor.[20,30] While **7** decomposed to SnO at 238 °C,[31] **3** shows negligible decomposition up to at least 275 °C by TGA, at which temperature the analyte had completely evaporated.

Despite its relatively lower volatility, **3** performed exceptionally well under realistic ALD process conditions, surviving over a week of continuous heating at 170 °C with no change in its thermal properties. We were able to reproduce the previously reported promising thermal behavior of **A**:[12] no films were deposited at 400 °C in a commercial ALD reactor after 2000 × 8 s pulses without an oxidizing co-reactant. This strongly suggests **1** and **2** can form a stable monolayer that is critical to ALD growth. The ease of synthesis and handling, high thermal stability, and good volatility make **3** a promising ALD precursor for F-doped SnO_2.

The dramatic difference in volatility among this family of compounds could not be explained by their enthalpies of vaporization: the temperature at which they reached 1 Torr of vapor pressure decreased from **8** (218 °C), **3** (191 °C), **7** (154 °C), to **5** (84 °C), while their ΔH_{vap} increased in the order **3** (72 kJ mol^{-1}), **7** (81 kJ mol^{-1}), **5** (83 kJ mol^{-1}), **8** (98 kJ mol^{-1}). One would expect **8**, a coordinately saturated complex of moderate molecular weight, to be more volatile than the polymeric compounds. But it was the least volatile by a large margin, reaching a pressure of 1 Torr at 134 °C higher than **5**. It is also surprising that **3** has the smallest ΔH_{vap} even though many O→Sn coordinative bonds must be broken to evaporate as **1** and **2**.

Of course, the Gibbs free energy of evaporation depends on the change in entropy ΔS as well as change in enthalpy ΔH, and the change in entropy of a system from condensed phase to the vapor phase is related to the number of possible microstates W available in that phase by the Boltzmann equation. Since vaporization is an endothermic process where $\Delta G \leq 0$, ΔH and ΔS must then both be positive. For highly symmetrical polymers like **5**, ΔS is large due to the depolymerization from one $(\mathbf{5})_n$ polymer into n gas phase monomers (naively, $W_g \sim nW_c$, where W_c represents the condensed phase, and W_g the gas phase), lowering the temperature required to satisfy $\Delta H \leq T\Delta S$. A similar argument can be made for the symmetrical polymer **7**,[27,28] but its lower vapor pressure is likely due to the secondary factor of increased intermolecular interactions between more polarizable CH_3 groups (when compared to CF_3).[27] The complexity and lability of **3** in the condensed phase lessens the difference between W_g and W_c, increasing the temperature required to satisfy the Gibbs inequality, decreasing its volatility. Similarly, the change in entropy upon vaporization of **8** is small due to its monomeric nature in the solid state[29] and gas phase. Overall, this suggests a new strategy in precursor design: volatility can be increased by forming

highly symmetrical coordination polymers to exploit their inherently large change in entropy upon evaporation into monomers.

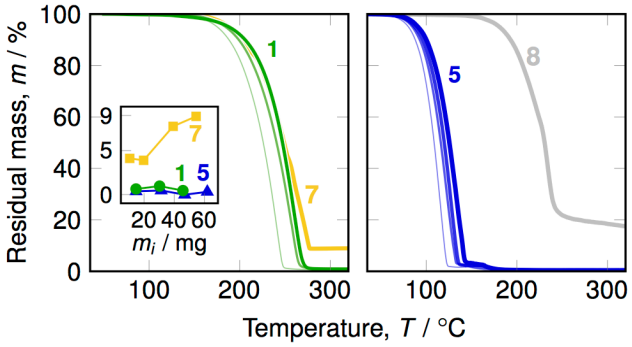

Figure 9. Ramped thermogravimetric analysis (TGA) curves of **3** (left, green), **7** (left, gold), **5** (right, blue) and **8** (right, gray). Stress tests (inset) reveal the stability of **3** (green circles) and **5** (blue triangles) with no increase in residual mass with increasing initial mass loading; and highlight the instability of **7** (gold squares) with a positive correlation. **8** was omitted as it decomposed considerably even at low mass loading (ca. 10 mg), so its comparison became trivial.

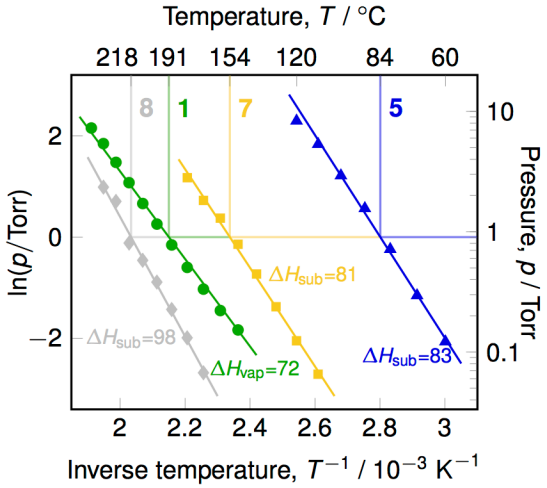

Figure 10. Vapor pressure of **1** (green circles), **7** (gold squares), **2** (blue triangles) and **8** (gray diamonds) as estimated by thermogravimetric analysis. Enthalpies (in kJ mol^{-1}) of evaporation (for **1**) and sublimation (**2**, **7**, and **8**) were estimated by the Clausius-Clapeyron equation.

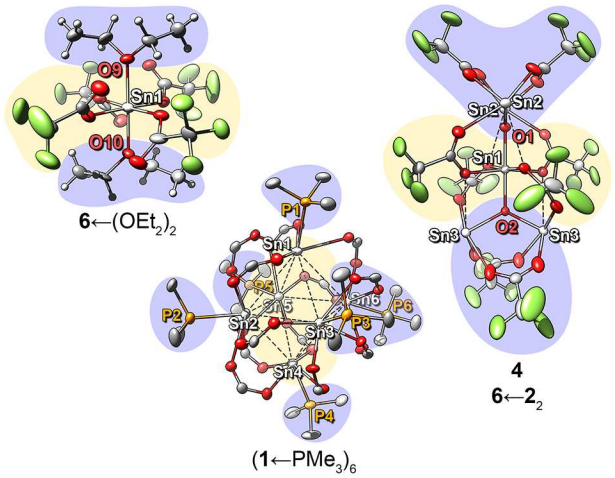

Figure 11. Molecular structures **6**←$(OEt_2)_2$ (left), (**1**←$PMe_3)_6$ (center), and **4** (right). Basic groups (i.e., Et_2O, **2**, and PMe_3) are highlighted in blue, and acidic groups (i.e., **1** and **6**) are highlighted in gold to show how **4** can be described as **6**←$\mathbf{2}_2$. Ellipsoids displayed at 50% probability; CF_3 groups and hydrogens are omitted from (**A**←$PMe_3)_6$ for clarity.

The variability in polymerization we found in **3** suggested that addition of additional Lewis bases could easily disrupt its structure. Exploiting this, we structurally characterized several other compounds and uncovered some patterns of tin trifluoroacetate supramolecular organization: the cage-like cluster hexakis[tin(II) bis(trifluoroacetate) trimethylphosphine] [(**1**←$PMe_3)_6$]; the anhydrous partial oxidation product of **3**, compound **4**;[15] and the diethyl ether σ-adduct **6**←$(OEt_2)_2$ (Figure 11). These are also similar to the previously reported mixed valence cluster ditin(II) ditin(IV) di-μ_3-oxy-octakis-μ-trifluoroacetate (**9**).[18] With these pieces we can complete the picture of supramolecular organization in the tin-oxy-trifluoroacetate system: Sn^{II} atoms adopt distorted square pyramidal five-coordinate geometries. Sn^{IV} atoms adopt octahedral geometries which distort upon coordination to Sn^{II} atoms. Homoleptic trifluoroacetates naturally act as Lewis acids, while trifluoroacetate groups bridge rather than chelate Sn centers to fill their coordination spheres, and bond more strongly to Sn^{IV} (bond lengths ca. 2.1 Å) than the more electron-rich Sn^{II} centers (bond lengths > 2.3 Å). Trifluoroacetic anhydride is apparently readily eliminated,[17,32,33] leaving

oxy moeties that donate σ-electron density to form basic Sn–O–Sn bridges and thus μ_3-oxy bridged Lewis pairs.

Together, **1**, **2**, **6**, and "$OSn^{IV}(O_2CCF_3)_2$" (**10**, the inferred trifluoroacetic anhydride elimination product of **6**) make up the elementary building blocks of tin-oxy-trifluoroacetate clusters and polymers. Consequently, **3** is more appropriately described as $(\mathbf{1}\leftarrow\mathbf{2})_\infty$, compound **4** as $\mathbf{6}\leftarrow\mathbf{2}_2$, and compound **9** as $(\mathbf{1}\leftarrow\mathbf{10})_2$. It is notable that **6** and **10** do not form a stable co-subliming complex like **1** and **2** do in **3**. If **9** is a typical example and **10** dimerizes like the central four-membered Sn_2O_2 heterocycle, then it is likely that intimate coordination between **6** and **10** is prevented by steric hinderance. The preparation and isolation of free **2** and **10** has not yet been successful, but the combination of these building blocks and other Lewis acids and bases opens a potentially versatile toolbox of thermally robust and amphoteric tin-containing supramolecular complexes.

Conclusion

Contrary to conventional wisdom, our results demonstrate that polymerization does not need to be avoided in precursor design if reversible thermal depolymerization can be achieved. In fact, it may increase the volatility over monomeric analogues. Despite its relatively lower volatility; the low cost, safe handling, and easy preparation of **3** make it the more attractive F-doped SnO_2 precursor for many applications. Compound **5** has potential as a complementary precursor for specialized application in very low temperature deposition. We are currently exploring processes using **3** or **5** as precursors to F-doped SnO_2 by ALD.

Experimental Details

General Synthetic Considerations

Most of the preparations reported below are oxygen- and moisture-sensitive, so they were performed under an inert atmosphere in a nitrogen-filled ("4.8" 99.998% purity) MBraun Labmaster 130 dry-box or under ultrapure nitrogen gas ("5.0" 99.999% purity) using standard Schlenk techniques. Those that can be performed under ambient conditions are noted as such. Low vacuum was achieved by a digitally regulated diaphragm pump (Buchi® VacoboxTM, min. ~10 Torr), and high vacuum by single-stage rotary vane pumps (Edwards RV5) whose absolute base pressures were measured to be 1-10 mTorr by a Hg-filled McLeod gauge. All solvents (e.g., toluene, hexanes, diethyl ether) were ACS Reagent grade or higher, degassed by an MBraun Solvent Purifier System using nitrogen gas ("4.8" 99.998% purity), and stored in a dry-box over freshly-regenerated 4 Å molecular sieves (Millipore-Sigma) for at least 24 h before use. Deuterated solvents were either used from a freshly opened ampoule, or degassed by three freeze-pump-thaw cycles then dried and stored over molecular sieves. Reverse osmosis water was deionized using a MilliQ system until its resistance reached 18 M . All purchased chemicals were used as received. Tin(II) oxide (≥95%), copper (II) oxide (powder, <10 μm, 98%), silver(I) oxide (ReagentPlus®, 99%), trifluoroacetic acid (ReagentPlus®, 99%), trifluoroacetic anhydride (ReagentPlus®, ≥99%), and tin(IV) bromide (99%) were purchased from Millipore-Sigma. Tin metal (powder, 100 mesh, 99.5%) was purchased from Strem Chemicals. Tin(II) diacetate,[31] tin(IV) tetraacetate,[34] silver(I) trifluoroacetate,[35] and copper(II) bis(2,2,6,6-tetramethylheptane-3,5-dionate)[36] [$Cu(tmhd)_2$] were prepared according to literature methods. Proton and heteronuclear NMR spectra were collected with a Bruker Avance II 300 MHz spectrometer at room temperature.

Synthetic Procedures

Caution! During experiments using trifluoroacetic acid, all ground glass fittings were sealed with PTFE thread. Silicone vacuum grease is very soluble in trifluoroacetic acid: prolonged reflux will lead to frozen joints and leaks, and filtration by inversion through a filter stick will allow trifluoroacetic acid to pass unimpeded through the glass joint, posing a serious safety risk due to acid burns from exposure to the vapour or liquid.

Hexatin(II) di-μ_3-oxy-octakis-μ-trifluoroacetate (3)

By oxidation of Sn^0 with $Cu^{II}(O_2CCF_3)_2$: Copper(II) bis(trifluoroacetate) was prepared in situ according to a modified literature method under ambient conditions.[37] One equivalent of copper(II) oxide (9.325 g, 116.0 mmol) was suspended in 200 mL water in a 500 mL round bottom flask with vigorous magnetic stirring. Two equivalents of trifluoroacetic acid (26.459 g, 232.1 mmol) was added in a continuous stream through an addition funnel. An exotherm occurred and the mixture was stirred with gentle (40 °C, overnight) or no heating (3 days) until it became azure blue and mostly transparent. The mixture was then filtered with suction through a Celite pad and a medium porosity fritted glass filter to remove unreacted CuO and other insoluble impurities to yield a clear azure blue solution. This was then deoxygenated by sparging for 30 min with a vigorous nitrogen flow through a fritted glass gas-diffusion tube.

Then, an excess of tin metal powder (27.548, 232.1 mmol) was added all at once to the aqueous $Cu(O_2CCF_3)_2$ solution under a stream of nitrogen gas at ambient temperature. Copper metal was clearly visible after an hour as shiny flakes, which were obscured after a day by redeposition of excess tin. Completion of the reaction was indicated by a fast settling, dark grey precipitate (Cu plated with Sn) and a colourless supernatant liquid, which was separated from the precipitate by filtration through a fritted glass filter stick under nitrogen to yield a colourless solution. Volatiles

were removed from the filtrate first by heating under low vacuum (~10 Torr, 60 °C, 4h) to yield a pale-yellow syrup that eventually becomes a colourless solid. This was dried with heating under high vacuum (1-10 mTorr, 100 °C, 8h) to yield 27.753 g of a colourless crystalline solid (87% crude yield based on CuO and HO_2CCF_3 used, assuming conversion to 1/6 eq. of **3**). Sublimation by vacuum-transfer (1-10 mTorr, 170 °C) into a cooled (−78 °C) receiving flask yielded **3** (26.120 g, 82% yield) as a colourless, sticky, amorphous solid that becomes a colourless crystalline solid that can be powdered upon cooling to −45 °C overnight. The title compound was deliquescent, and must be stored dry, although dry O_2 does not appear to degrade samples. Oxidation occurs slowly and **1** can be briefly handled under ambient conditions. It was very soluble in coordinating solvents (e.g., THF, ACN, DMSO), and slightly soluble in aromatic hydrocarbons. It forms a stable solution in water in the absence of O_2, showing no hydrolysis. M.p. 127 °C, sublimed. Crystals suitable for X-ray crystallography were grown by slow cooling of a toluene solution of **1** that was previously sublimed twice. HRMS (EI^+): Found *m*/*z* = 578.7624, calculated $Sn_2(O_2CCF_3)_3$ 578.7595, dev. 2.69 mmu; *m*/*z* = 481.7718, calc. $Sn_2O(O_2CCF_3)_2$ 481.7694, dev. 2.40 mmu; *m*/*z* = 364.7866, calc. $Sn_2O(O_2CCF_3)$ 364.7867, dev. 0.1 mmu; *m*/*z* = 276.8633, calc. $Sn(O_2CCF_3)CO_2$ 276.8771, dev. 13.8mmu. NMR chemical shifts of **3** in D_3CCN, (δ_0 = 1.94 ppm): silent; $^{13}C\{^1H\}$ (δ_0 = 1.32 ppm): 117.03 ppm (*q*, O_2CCF_3, $^1J_{C-F}$ = 288 Hz), 162.19 ppm (*q*, O_2CCF_3, $^2J_{C-F}$ = 38.7 Hz); ^{19}F (external reference, HO_2CCF_3 in D_2O δ_0 = −75.15 ppm): −75.61 ppm (*s*). ^{119}Sn (external reference, $Sn[N(SiMe_3)_2]_2$ in C_6D_6 δ_0 = 770 ppm): silent. *(Note: the combined effects of dynamic solvent exchange and compounded* $^2J_{Sn-C}$, $^2J_{119Sn-119Sn}$, $^2J_{119Sn-117Sn}$, $^3J_{Sn-C}$, *and* $^4J_{Sn-F}$ *coupling likely led to extreme broadening of the signal to the point where it could not be detected.)*

Condensation of SnO with trifluoroacetic acid was performed according to a modified literature procedure.[15] Blue-black tin(II) oxide (6.310 g, 46.84 mmol) was placed in a 250 mL Schlenk flask

and dried under high vacuum (10 mTorr) at room temperature for 3 h. The flask was refilled with nitrogen and fitted with a water-cooled reflux condenser, previously flamed-dried under vacuum, closed with a rubber sepctum. One equivalent of trifluoroacetic anhydride (9.838 g, 46.84 mmol) in a large excess of trifluoroacetic acid (100 mL, 760 mmol) was deoxygenated by three freeze-pump-thaw cycles, then cannulated onto the SnO through the condenser. The mixture was heated to reflux with vigorous stirring under nitrogen for eight days, then cooled to room temperature to yield a colourless supernatant liquid and a sticky beige precipitate. This mixture was filtered through a fritted glass filter stick under nitrogen to yield a colourless solution. The filtrate was worked up and purified in a manner identical to the one detailed above to yield a colourless solid (11.676 g, 85% yield assuming conversion to **3**) that had identical thermal and spectroscopic characteristics to the material prepared by redox.

*Hexakis[tin(II) bis-*μ*-trifluoroacetate trimethylphosphine] [(**1**←PMe_3)$_6$]:* Compound **3** (1.000 g, 0.6066 mmol) was suspended in toluene (10 mL) and trimethylphosphine (0.221 g, 2.90 mmol, in 10 mL toluene) was added dropwise resulting in a clear colorless solution. (The PMe_3 was added in excess due to our presumption that the starting material was **1**, M = 344.74 g/mol, before we discovered it was **1**.) Crystals of (**A**←PMe_3)$_6$ were grown by slow cooling this solution to −45 °C for a week.

Tetratin(II) monotin(IV) di-μ_3*-oxy-octakis-*μ*-trifluoroacetate (**4**):* Crystals of **4** were grown by placing a sample of **3** (∼100 mg) in a PTFE-capped O-ring sealed glass pressure vessel in a dry-box and heating in an oven at 200 °C for 2 h until the sample had completely evaporated. Heating was stopped, and the oven was allowed to cool slowly. Large sticky crystals (presumably **3**) were deposited throughout the vessel but could not be successfully harvested. Smaller cubic crystals of **4** suitable for crystallography were found near the cap of the vessel.

Tin(IV) tetrakis(trifluoroacetate) (5)

Acidolysis of tetraphenyltin was performed according to a known literature procedure with modified workup.[38] Tetraphenyltin (4.271 g, 10.00 mmol) was placed in a 250 mL Schlenk flask, then degassed and dried under high vacuum at room temperature for one hour. One equivalent of trifluoroacetic anhydride (2.100 g, 10.00 mmol) in a large excess of trifluoroacetic acid (100 mL) was cannulated into the flask. The suspension was stirred until it became a clear green/tan solution (about 1 day), then the volatiles were removed at ambient temperature under high vacuum. The resulting pale yellow/green solid was purified by vacuum transfer (10 mTorr, 60 °C) to yield a colourless crystalline solid contaminated with a less volatile by-product (observed by TGA) believed to be the product upon elimination of trifluoroacetic anhydride (i.e., "$SnO(O_2CCF_3)_2$", **10**). The solid was sublimed again (10 mTorr, 60 °C) to yield **2** (3.140 g, 55% based on Ph_4Sn, m.p. 115 °C, lit. 114-115 °C[38]) as a colourless crystalline and very moisture-sensitive solid. Compound **2** is very soluble in trifluoroacetic acid, coordinating aprotic solvents, and moderately soluble in aromatic hydrocarbons. Solutions of **5** fume when exposed to ambient conditions, but the solid can be briefly handled in air without significant hydrolysis. Crystals suitable for X-ray crystallography were grown by sublimation: **5** (250 mg) was placed in a PTFE-capped O- ring sealed glass pressure vessel in a glove box and placed on top of an oven in a warm zone at approximately 50 °C. After about 3 weeks, crystals of **5** deposited on the cooler end of the vessel. Crystals of the bis(etherate) were grown by slow cooling to –45 °C of a solution of **2** in 1:1 diethyl ether/pentane, after 2 days crystals of **C**←$(OEt_2)_2$ were deposited.

Thermogravimetric Analysis (TGA)

TGA was performed on Pt pans with a TA Instruments Q50 housed in an MBraun Labmaster 130 dry-box filled with nitrogen gas ("4.8" 99.998% purity). Pt pans were cleaned by sequential

ultrasonication in dilute nitric acid (~3 N), water, then 2-propanol. They were then heated until red hot by a propane torch flame in air to remove remaining impurities. Ramp experiments were performed under a flow of ultrapure nitrogen ("5.0" 99.999% purity, 60 sccm) at 10 °Cmin^{-1} to a maximum temperature of 500 °C. Stress-tests were performed under the same conditions sequentially on freshly cleaned pans with incrementally increasing initial mass loadings.

Vapour pressures were estimated using a modified literature method.[39] Vaporization constants α (from the Langmuir equation) were obtained for our instrument by calibrating compounds with known Antoine equation parameters and volatilities similar to the analyte. Benzoic acid (α_{loT} = 2.016×10^{-4}) was used for high volatility compounds (i.e., **5**), and $Cu(tmhd)_2$[40] ($\alpha_{hiT} = 4.512 \times 10^{-5}$) was used for low volatility compounds (i.e., **1**, **7**, **8**). The temperature program was set to jump by increments of 10 °C, then hold that temperature for 7 minutes to allow the evaporating system to reach equilibrium, and then the derivative of mass with respect to temperature dm/dT was taken from the linear regions of the isotherm steps for each temperature. These data were used to find the pressure p as a function of T, thus ln p as a function of T^{-1}, which can be modeled with the Clausius-Clapeyron equation. The slope of this line is equal to the enthalpy of sublimation (before melting) and evaporation (after melting) divided by the gas constant $\Delta H/R$.

Evaluation of Atomic Layer Deposition (ALD) Potential of 1

The potential for **3** to form a thermally stable self-limiting monolayer under operando ALD conditions was evaluated in a commercial Picosun R-150 hot-wall viscous flow ALD reactor. Powdered samples of **3** (up to 10 g) were loaded into an open-cup glass-lined stainless steel bubbler in a dry-box, capped with a rubber septum, then loaded into the bubbler heating jacket under a strong flow of ultrapure nirogen ("5.0" 99.999%, 250 sccm). The bubbler and lines were evacuated to the base operating pressure of the reactor (ca. 10 hPa) to remove any water or oxygen that may

have become trapped in the bubbler during loading. Then the bubbler and delivery lines were heated to 170 °C for 1 h before deposition to allow the precursor to melt and heat evenly. Precursor vapour was delivered into the deposition chamber with a "pulse": two pneumatic ALD valves were opened between the carrier gas inlet, the precursor, and the reactor, and nitrogen carrier gas was flowed over the heated precursor at 200 sccm for 8 s under active vacuum, after which the valves were closed in reverse order. The lines and reactor chamber were purged with nitrogen carrier gas at 150 sccm for 8 s to remove any unreacted **3** vapour and by-products of its self-assembly into a molecular layer on the surface.

During evaluation, several substrates were loaded into the deposition chamber: single-side polished "mechanical grade" high-purity hydrogen terminated single-crystalline (100) Si (RCA cleaned, sonicated in 2% HF (aq) for 30 min immediately prior to use), 100 nm Al_2O_3 films (deposited by 900 cycles of ALD using trimethylaluminum and water at 250 °C on bare Si), 100 nm SiO_2 (thermally grown on Si at 1200 °C in O_2) and soda-lime glass microscope slides (cleaned by sonication for 30 min each in acetone, 2-propanol, and deionized water). No films could be observed after 2000 pulses of **1** at a reactor temperature of 400 °C by eye (evident as interference patterns on reflective, and colour changes on transparent substrates), ellipsometry or scanning electron microscopy (SEM). Preliminary ALD experiments using an oxidizing co-reagent (e.g., air) deposited uniform and transparent films. Above 420 °C, an uncharacterized patchy mottled blue-grey material was observed on all substrates without co-reagent, indicating CVD growth behavior and the absence of ALD-like growth.

X-ray Crystallography

Crystals were attached to the tip of an appropriately sized μm MicroLoop with Paratone-N oil. Measurements were made on a Bruker APEXII CCD equipped diffractometer (30 mA, 50 mV)

using monochromated Mo Kα radiation (λ = 0.71073 Å) at 125 K. APEX2 software[41] was used for the initial orientation and unit cells were indexed using a least-squares analysis of a random set of reflections collected from three series of 0.5° wide scans, 10 seconds per frame and 12 frames per series that were well distributed in reciprocal space. For data collection, four ω-scan frame series were collected with 0.5° wide scans, 5 seconds frames and 366 frames per series at varying φ angles (φ = 0°, 90°, 180°, and 270°). The crystal-to-detector distance was set to 6 cm and a complete sphere of data was collected. Cell refinement and data reduction were performed with the Bruker APEX3 software, which corrects for beam inhomogeneity, possible crystal decay, Lorentz and polarization effects. Data processing and a multi-scan absorption correction was applied using the APEX3 software package.[42] The structure was solved using intrinsic phasing[43] and all non-hydrogen atoms were refined anisotropically using SHELXL[44] using a combination of the shelXle graphical user interface[45] and OLEX^2.[46] Figures were made using UCSF Chimera[47] and Adobe Photoshop CC 2018. CCDC 1885252-1885256 contains the supplementary crystallographic data for complexes **3**, **5**, (**1**←$PMe_3)_6$, **6**←$(OEt_2)_2$, and **4**, respectively. These data can be obtained free of charge from the Cambridge Crystallographic Database Centre via https://summary.ccdc.cam.ac.uk/structure- summary-form.

Hexatin(II) di-μ_3*-oxy-octakis-*μ*-trifluoroacetate (**3**):* Two $-CF_3$ groups were found to be best modeled using a two-component disorder model, one in a 66:34 ratio (on C8) and the other in a 73:27 (on C14). Details of crystal data, data collection, and structure refinement are listed in Table S1.

*Tin(IV) tetrakis(trifluoroacetate) (**5**):* One of the CF_3 groups was modeled with a two-component disorder model in a 53:47 ratio. Details of crystal data, data collection, and structure refinement are listed in Table S4.

Hexakis[tin(II) bis-μ-*trifluoroacetate trimethylphosphine] [(**1**←$PMe_3)_6$]:* One CF_3 exhibited three-position disorder (53:33:14). Other CF_3 groups had larger thermal parameters, but attempts to model the disorder did not yield better models so they were left as is. One toluene molecule was found in the difference map and was successfully modelled. Another toluene model was found but attempts at modelling failed; the SQUEEZE routine was used and 48 electrons were removed, closely matching the expected 50 electrons for a toluene molecule. Details of crystal data, data collection, and structure refinement are listed in Table S6.

Tin(IV) tetrakis(trifluoroacetate)-trans-*bis(diethyl ether) [**6**←$(OEt_2)_2$]:* Details of crystal data, data collection, and structure refinement are listed in Table S9.

Tetratin(II) monotin(IV) di-μ_3-*oxy-octakis*-μ-*trifluoroacetate (**4**):* This compound was found to be a two-component inversion twin and was treated appropriately. Details of crystal data, data collection, and structure refinement are listed in Table S12.

Theoretical Calculations

All theoretical calculations were carried out using the Gaussian09 Rev.D01[48] software suite. All geometry optimizations of $Sn(O_2CCF_3)_2$ (**1**) and $Sn_2O(O_2CCF_3)_2$ (**2**) were performed in the C_2 symmetry point group, and $Sn(O_2CCF_3)_4$ (**6**) was performed in the D_{2d} symmetry point group. The highest-level geometry optimizations accounted for scalar relativistic effects using the 2nd-order Douglas-Kroll-Hess (DKH) Hamiltonian[49–52] and employed the SOGGA11-X[53] density functional of Truhlar and Peverati, coupled with the all electron double-ζ and triple-ζ-quality DZP-DKH and TZP-DKH basis sets of Jorge et al..[54–56] The point-nuclei model was used in the DKH treatment.

To establish flexible restraints for use in a SARACEN[57–59] GED refinement, additional optimizations were carried out using the M06,[60] M11,[61] and SOGGA11-X[53] density functionals coupled with the *def* 2-SVP, *def* 2-TZVP, and *def* 2-QZVP basis sets.[62,63] The characters of all

optimized geometries were verified via vibrational frequency analysis and were confirmed to correspond to minima on the ground-state potential energy surface. Cartesian coordinates of all optimized geometries are found in Tables S18-S39 (for **1** and **2**) and Tables S48-S58 (for **C**). Theoretical r_{h1}-type amplitudes of vibration (u_{h1}) and curvilinear distance corrections (k_{h1}) were generated for **1**, **2**, **6** from force fields computed at the SOGGA11-X/*def* 2-SVP level using the SHRINK software package.[64,65]

Gas-phase Electron Diffraction (GED)

GED data for **1**, **2**, and **6** were acquired using the University of York gas electron diffractometer.[66] An accelerating potential of 42.22 kV was applied to produce an electron emission current of 0.66 μA and an electron wavelength of ca. 5.85 pm. The scattered electrons were recorded via exposures of image plates (Fuji BAS-IP MS 2025) at nozzle-to-image-plate distances of 234.5 and 477.0 mm for **1** and **2** and at nozzle-to-image-plate distances of 233.5 and 486.0 mm for **6**. Five exposures were recorded at each nozzle-to-image-plate distance. To acquire data for **1** and **2**, the sample and the nozzle were heated to 463 and 473 K, respectively, during exposures at both nozzle-to-image-plate distances. To acquire data for **6**, the sample and the nozzle were heated to 398 and 403 K, respectively, during exposures at both nozzle-to-image-plate distances. A flatbed image plate scanner (Fuji BAS-1800II) was used to digitize the scattering intensities recorded on the image plates. Summaries of the experimental conditions used to acquire data for **1** and **2**, and **6**, can be found in Tables S17 and S47, respectively.

Reduction and Refinement

Digitized diffraction patterns were reduced to molecular intensity curves (MICs) using the data extraction package *xtract*.[67] MICs were refined using the ed@ed v3.0 least-squares refinement package,[68] employing the electron scattering factors of Ross et al.[69]

The least-squares refinement procedures employed parameterized molecular models: one de- scribing both **1** and **2**, each within the C_2 symmetry point group, in terms of 23 refinable parameters comprising 11 distances (p_1-p_{11}), 5 angles (p_{12}-p_{14}, p_{19}, and p_{23}) and 7 dihedral angles (p_{15}-p_{18} and p_{20}-p_{22}) with the option to weight the fraction of each **1** and **2**, and one describing **6** within the D_{2d} symmetry point group in terms of 12 refinable parameters comprising 8 distances (p_1-p_8) and 4 angles (p_9- p_12). Definitions of the refinable parameters used for **1** and **2**, and **6**, are given in Tables S40 and S59, respectively. The FORTRAN90 code for the parametrized molecular models is available free-of-charge at DOI: 10.15124/5cb0c982-b280-47e9-9d46-08e675dfe0af.

The least-squares refinement procedures used the SARACEN approach and yielded internuclear distances of the r_{h1} type; r_{h1}-type internuclear distances are related to the vibrationally-averaged r_a-type distances determined directly via the GED experiment by the relationship $r_{a3} \approx r_a + u_h{}^2{}_1/r_a - k_{h1}$. SARACEN restraints were centered on values obtained from geometry optimizations at the SOGGA11-X/TZP-DKH level. For the refinement of **1** and **2**, and for the refinement of **6**, restraints were applied to 9 of the 23, and 7 of the 12, parameters, respectively, with the remaining parameters being allowed to refine free from restraint. 7 parameters remained unrefined after finalizing the refinement of **1** and **2**; no parameters remained unrefined after finalizing the refinement of **6**. Estimates of the uncertainties associated with the SARACEN restraint values were derived from sequential geometry optimizations using the M06, M11, and SOGGA11-X density functionals coupled with the *def* 2-SVP, *def* 2-TZVP, and *def* 2-QZVP basis sets.

The weighting points for off-diagonal weight matrices, scaling factors, and correlation parameters associated with the refinement of **1** and **2**, and with the refinement of **6**, can be found in Tables S41 and S60, respectively. Summaries of the refined (r_{h1}-type) and theoretical (r_e-type,

SOGGA11-X/TZP-DKH) parameters p_1 to p_{23} (describing **1** and **2**), and parameters p_1 to p_{12} (describing **6**) — accompanied, in each case, by uncertainties — can be found in Tables S42 and S61, respectively. Correlation matrices can be found in Tables S43 and S62, respectively. All amplitudes of vibration were refined as outlined in Ref. 36. Summaries of internuclear distances, refined and theoretical amplitudes of vibration, r_{h1}-type distance corrections, and SARACEN restraints (where applied) are tabulated for **1** and **2** in Table S44 and for **6** in Table S63. Cartesian coordinates for the refined geometries of **1**, **2**, and **6** are found in Tables S45, S46, and S64, respectively.

Supporting Information Available

Crystallographic data for **3**, **4**, **5**, [**1**←PMe_3]$_6$, and **6**←$(OEt_2)_2$ (CCDC 1885252-1885256). GED determined structures of **1**, **2** and **6** (*.xyz* format). Electron-impact (EI) and electrospray ionization (ESI) mass spectrograms of **3** (Figures S1-2), radial distribution curves (RDC) and molecular intensity curves (MIC) from GED of **1** and **2** and **6** (Figure S3-5). Crystallographic Figures and Tables (Figures S4-S11, Tables S0-S16). Cartesian coordinates and energies of DFT-optimized geometries (Tables S18-S39 and S48-S58), summary of fixed (nonrefinable) parameter values (Tables S40 and S59), summary of GED experimental parameters (Tables S41 and S60), a summary of refined and theoretical refinable parameter values with SARACEN restraints (Tables S42 and S61), least squares correlation matrix (Tables S43 and S62), r_a-type internuclear distances, refined and theoretic amplitudes of vibration and distance corrections with SARACEN restraints (Tables S44 and S63), and the refined Cartesian coordinates for the GED-determined structure (Table S45-S46 and S64) of **1** and **2**, and **6**, respectively.

Acknowledgements

We wish to thank Dr. Sharon Curtis at the University of Ottawa for mass spectrometry, and Tomas Lock Feixas and Justas Benetis for assisting with GED data acquisition. G.B. and S.T.B. acknowledge the QEII-OGSST program for funding and Carleton University for support. J.D.M. thanks NSERC for funding in the form of a Discovery Grant (RGPIN-2015-03825) and acknowledges the Canada Foundation for Innovation (CFI) and Nova Scotia Research and Innovation Trust Fund for equipment funding (CFI/30368). D.A.W. thanks EPSRC for funding his fellowship (EP/I004122) and C.D.R. thanks EPSRC for funding his studentship (EP/1651146). All GED and DFT data created during this research are available by request from the University of York Data Catalogue (DOI: 10.15124/5cb0c982-b280-47e9-9d46-08e675dfe0af).

References

(1) Kumar, A.; Zhou, C. The Race to Replace Tin-Doped Indium Oxide: Which Material Will Win? *ACS Nano* **2010**, *4* (1), 11–14.

(2) Ellmer, K. Past Achievements and Future Challenges in the Development of Optically Transparent Electrodes. *Nat. Photonics* **2012**, *6* (12), 809.

(3) Gordon, R. G. Criteria for Choosing Transparent Conductors. *MRS Bull.* **2000**, *25* (8), 52–57.

(4) Andersson, A.; Johansson, N.; Bröms, P.; Yu, N.; Lupo, D.; Salaneck, W. R. Fluorine Tin Oxide as an Alternative to Indium Tin Oxide in Polymer LEDs. *Adv. Mater.* **1998**, *10* (11), 859–863.

(5) George, S. M. Atomic Layer Deposition: An Overview. *Chem. Rev.* **2009**, *110* (1), 111–131.

(6) Miikkulainen, V.; Leskelä, M.; Ritala, M.; Puurunen, R. L. Crystallinity of Inorganic Films Grown by Atomic Layer Deposition: Overview and General Trends. *J. Appl. Phys.* **2013**, *113*, 1. https://doi.org/10.1063/1.4757907.

(7) Choi, Y.-J.; Park, H.-H. A Simple Approach to the Fabrication of Fluorine-Doped Zinc Oxide Thin Films by Atomic Layer Deposition at Low Temperatures and an Investigation into the Growth Mode. *J. Mater. Chem. C* **2014**, *2* (1), 98. https://doi.org/10.1039/c3tc31478b.

(8) Lee, Y.; Sun, H.; Young, M. J.; George, S. M. Atomic Layer Deposition of Metal Fluorides Using HF--Pyridine as the Fluorine Precursor. *Chem. Mater.* **2016**, *28* (7), 2022–2032.

(9) Pilvi, T.; Puukilainen, E.; Kreissig, U.; Leskelä, M.; Ritala, M. Atomic Layer Deposition of \ce{MgF2} Thin Films Using \ce{TaF5} as a Novel Fluorine Source. *Chem. Mater.*

2008, *20* (15), 5023–5028.
(10) Putkonen, M.; Szeghalmi, A.; Pippel, E.; Knez, M. Atomic Layer Deposition of Metal Fluorides through Oxide Chemistry. *J. Mater. Chem.* **2011**, *21* (38), 14461–14465. https://doi.org/10.1039/c1jm11825k.
(11) Boutonnet, J. C.; Bingham, P.; Calamari, D.; Rooij, C. de; Franklin, J.; Kawano, T.; Libre, J.-M.; McCul-loch, A.; Malinverno, G.; Odom, J. M.; et al. Environmental Risk Assessment of Trifluoroacetic Acid. *Hum. Ecol. Risk. Assess.* **1999**, *5* (1), 59–124.
(12) Maruyama, T.; Tabata, K. Fluorine-Doped Tin Dioxide Thin Films Prepared by Chemical Vapor Deposition. *J. Appl. Phys.* **1990**, *68* (8), 4282–4285.
(13) Korotkov, R. Y.; Ricou, P.; Farran, A. J. E. Preferred Orientations in Polycrystalline \ce{SnO2} Films Grown by Atmospheric Pressure Chemical Vapor Deposition. *Thin Solid Films* **2006**, *502* (1–2), 79–87.
(14) Belanger, D.; Dodelet, J. P.; Lombos, B. A.; Dickson, J. I. Thickness Dependence of Transport Properties of Doped Polycrystalline Tin Oxide Films. *J. Electrochem. Soc.* **1985**, *132* (6), 1398–1405.
(15) Birchall, T.; Faggiani, R.; Lock, C. J. L.; Manivannan, V. Preparation and Partial Oxidation of Tin (II) Trifluoroacetate: Spectroscopic Properties and X-Ray Crystal Structure of Di-\ce{\mu_3} -Oxo-Octakis-\ce{\mu}-Trifluoroacetato-Tetratin (II) Tin (IV). *J. Chem. Soc., Dalt. Trans.* **1987**, No. 7, 1675–1682.
(16) Batchelor, R. J.; Birchall, T.; Johnson, J. P. The Crystal Structure of \ce{Sn6O2(CF3CO2)8*CF3CO2H}. *Can. J. Chem.* **1987**, *65* (9), 2187–2193.
(17) Birchall, T.; Johnson, J. P. Crystal Structure of Di-\ce{\mu_3}-Oxo-Octakis-\ce{\mu}-(Trifluoroacetato)-Ditin (II) Ditin (IV)--Benzene (1/1). *J. Chem. Soc., Dalt. Trans.* **1981**, No. 1, 69–73.
(18) Zabula, A. V; Filatov, A. S.; Petrukhina, M. A. Coordinatively Unsaturated Polynuclear Mixed-Valent \ce{Sn^{II}}--\ce{Sn^{IV}} and \ce{Cu^{II}}--\ce{Sn^{IV}} Oxo-Centered Carboxylates. *J. Clust. Sci.* **2010**, *21* (3), 361–370.
(19) Daly, S. R.; Kim, D. Y.; Girolami, G. S. Lanthanide N,N-Dimethylaminodiboranates as a New Class of Highly Volatile Chemical Vapor Deposition Precursors. *Inorg. Chem.* **2012**, *51* (13), 7050–7065. https://doi.org/10.1021/ic201852j.
(20) Coyle, J. P.; Sirianni, E. R.; Korobkov, I.; Yap, G. P. A.; Dey, G.; Barry, S. T. Study of Monomeric Copper Complexes Supported by N-Heterocyclic and Acyclic Diamino Carbenes. *Organometallics* **2017**, *36* (15), 2800–2810.
(21) Cheng, Y.; Emge, T. J.; Brennan, J. G. Polymeric \ce{Cd(Se{-}2{-}NC5H4)2} and Square Planar \ce{Hg(Se{-}2{-}NC5H4)2}: Volatile CVD Precursors to II-VI Semiconductors. *Inorg. Chem.* **1994**, *33* (17), 3711–3714.
(22) Donaldson, J. D.; Moser, W. 789. Pure Tin (II) Sulphate. *J. Chem. Soc.* **1960**, 4000–4003.
(23) Anastas, P. T.; Zimmerman, J. B. Peer Reviewed: Design Through the 12 Principles of Green Engineering. *Environ. Sci. Technol.* **2003**, *37* (5), 94A-101A.
(24) Gao, Y.; Yang, Y.; Zheng, W.; Su, Y.; Zhang, X.; Roesky, H. W. Germanium and Tin Monoxides Trapped by Oxophilic Germylene and Stannylene Ligands. *Inorg. Chem.* **2017**, *56* (17), 10220–10225.
(25) Weimer, M. S.; Hu, B.; Kraft, S. J.; Gordon, R. G.; Segre, C. U.; Hock, A. S. Synthetic and Spectroscopic Study of the Mechanism of Atomic Layer Deposition of Tin Dioxide. *Organometallics* **2016**, *35* (9), 1202–1208.
(26) Mackus, A. J. M.; MacIsaac, C.; Kim, W.-H.; Bent, S. F. Incomplete Elimination of

Precursor Ligands during Atomic Layer Deposition of Zinc-Oxide, Tin-Oxide, and Zinc-Tin-Oxide. *J. Chem. Phys.* **2017**, *146* (5), 52802.
(27) Stafeeva, V. S.; Mitiaev, A. S.; Abakumov, A. M.; Tsirlin, A. A.; Makarevich, A. M.; Antipov, E. V. Crystal Structure and Chemical Bonding in Tin (II) Acetate. *Polyhedron* **2007**, *26* (18), 5365–5369.
(28) Smart, B. A.; Griffiths, L. E.; Pulham, C. R.; Robertson, H. E.; Mitzel, N. W.; Rankin, D. W. H. Molecular Structure of Tin (II) Acetate as Determined in the Gas Phase by Electron Diffraction and Ab Initio Calculations. *J. Chem. Soc., Dalt. Trans.* **1997**, No. 9, 1565–1570.
(29) Alcock, N. W.; Tracy, V. L. Acetates and Acetato Complexes. IV. The Crystal and Molecular Structure of Tin Tetraacetate. *Acta Crystallogr., Sect. B Struct. Crystallogr. Cryst. Chem.* **1979**, *35* (1), 80–83.
(30) Bačić, G.; Zanders, D.; Mallick, B.; Devi, A.; Barry, S. T. Designing Stability into Thermally Reactive Plumbylenes. *Inorg. Chem.* **2018**, *57* (14), 8218–8226.
(31) Donaldson, J. D.; Moser, W.; Simpson, W. B. 1147. Tin (II) Acetates. *J. Chem. Soc.* **1964**, 5942–5947.
(32) Sartori, P.; Weidenbruch, M. Trifluoroacetates of Silicon, Germanium, and Tin. *Angew. Chem., Int. Ed. Engl.* **1965**, *4* (12), 1079.
(33) Sartori, P.; Weidenbruch, M. Über Die Darstellung Und Eigenschaften von Perfluoracyloxy-Verbindungen Der Vierten Gruppe Des Periodensystems. *Chem. Ber.* **1967**, *100* (6), 2049–2063.
(34) Sawyer, A. K.; Frey, C. A Simple Synthesis of Tin(IV) Acetate from Tetraphenyltin. *Synth. React. Inorg. Met.-Org. Chem.* **1983**, *13* (2), 259–262.
(35) Janssen, D. E.; Wilson, C. V. 4-Iodoveratrole. *Org. Synth.* **1963**, *36*, 46.
(36) Rees, W. S.; Carris, M. W.; Girolami, G. S.; You, Y. Bis(2,2,6,6-Tetramethyl-3,5-Heptanedionato) Copper. In *Inorg. Synth.*; John Wiley & Sons, Ltd, 2007; pp 286–288.
(37) Cotton, F. A.; Dikarev, E. V; Petrukhina, M. A. Syntheses and Crystal Structures of ``Unligated'' Copper(I) and Copper(II) Trifluoroacetates. *Inorg. Chem.* **2000**, *39* (26), 6072–6079.
(38) Birchall, T.; Johnson, J. P. Preparation and Characterization of Mixed-Oxidation-State Tin Carboxylates and Related Tin (IV) Carboxylates. *Inorg. Chem.* **1982**, *21* (10), 3724–3731.
(39) Kunte, G. V; Shivashankar, S. A.; Umarji, A. M. Thermogravimetric Evaluation of the Suitability of Precursors for MOCVD. *Meas. Sci. Technol.* **2008**, *19* (2), 25704.
(40) Colominas, C.; Lau, K. H.; Hildenbrand, D. L.; Crouch-Baker, S.; Sanjurjo, A. Vapor Pressures of the Copper and Yttrium $β$-Diketonate MOCVD Precursors. *J. Chem. Eng. Data* **2001**, *46* (2), 446–450.
(41) Bruker. No Title. In *APEX2 v2008.5*; Bruker AXS, Madison, Wisconsin, USA, 2008.
(42) Bruker. No Title. In *APEX3 v2016.1-0*; Bruker AXS, Madison, Wisconsin, USA, 2016.
(43) Sheldrick, G. M. SHELXT--Integrated Space-Group and Crystal-Structure Determination. *Acta Crystallogr. A* **2015**, *71* (1), 3–8.
(44) Sheldrick, G. M. Crystal Structure Refinement with SHELXL. *Acta Crystallogr. C* **2015**, *71* (1), 3–8.
(45) Hübschle, C. B.; Sheldrick, G. M.; Dittrich, B. ShelXle: A Qt Graphical User Interface for SHELXL. *J. Appl. Crystallogr.* **2011**, *44* (6), 1281–1284.
(46) Dolomanov, O. V; Bourhis, L. J.; Gildea, R. J.; Howard, J. A. K.; Puschmann, H. OLEX2: A Complete Structure Solution, Refinement and Analysis Program. *J. Appl. Crystallogr.*

2009, *42* (2), 339–341.
(47) Pettersen, E. F.; Goddard, T. D.; Huang, C. C.; Couch, G. S.; Greenblatt, D. M.; Meng, E. C.; Ferrin, T. E. UCSF Chimera--a Visualization System for Exploratory Research and Analysis. *J. Comput. Chem.* **2004**, *25* (13), 1605–1612.
(48) Frisch, M. J.; Trucks, G. W.; Schlegel, H. B.; Scuseria, G. E.; Robb, M. A.; Cheeseman, J. R.; Scalmani, G.; Barone, V.; Mennucci, B.; Petersson, G. A.; et al. Gaussian~09 {R}evision {D}.01.
(49) Douglas, M.; Kroll, N. M. Quantum Electrodynamical Corrections to the Fine Structure of Helium. *Ann. Phys.* **1974**, *82* (1), 89–155.
(50) Hess, B. A. Applicability of the No-Pair Equation with Free-Particle Projection Operators to Atomic and Molecular Structure Calculations. *Phys. Rev. A* **1985**, *32* (2), 756.
(51) Hess, B. A. Relativistic Electronic-Structure Calculations Employing a Two-Component No-Pair Formalism with External-Field Projection Operators. *Phys. Rev. A* **1986**, *33* (6), 3742.
(52) Jansen, G.; Hess, B. A. Revision of the Douglas-Kroll Transformation. *Phys. Rev. A* **1989**, *39* (11), 6016–6017.
(53) Peverati, R.; Truhlar, D. G. Communication: A Global Hybrid Generalized Gradient Approximation to the Exchange-Correlation Functional That Satisfies the Second-Order Density-Gradient Constraint and Has Broad Applicability in Chemistry. *J. Chem. Phys.* **2011**, *135* (19), 191102.
(54) Jorge, F. E.; Neto, A. C.; Camiletti, G. G.; Machado, S. F. Contracted Gaussian Basis Sets for Douglas{\textendash}Kroll{\textendash}Hess Calculations: Estimating Scalar Relativistic Effects of Some Atomic and Molecular Properties. *J. Chem. Phys.* **2009**, *130* (6), 64108.
(55) Barros, C. L.; de Oliveira, P. J. P.; Jorge, F. E.; Neto, A. C.; Campos, M. Gaussian Basis Set of Double Zeta Quality for Atoms Rb through Xe: Application in Non-Relativistic and Relativistic Calculations of Atomic and Molecular Properties. *Mol. Phys.* **2010**, *108* (15), 1965–1972.
(56) Campos, C. T.; Jorge, F. E. Triple Zeta Quality Basis Sets for Atoms Rb through Xe: Application in {CCSD}(T) Atomic and Molecular Property Calculations. *Mol. Phys.* **2012**, *111* (2), 167–173.
(57) Mitzel, N. W.; Smart, B. A.; Blake, A. J.; Robertson, H. E.; Rankin, D. W. H. Conformational Analysis of 1, 4-Disilabutane and 1, 5-Disilapentane by Combined Application of Gas-Phase Electron Diffraction Andab {InitioCalculations} and the Crystal Structure of 1, 5-Disilapentane at Low Temperatures. *J. Phys. Chem.* **1996**, *100* (22), 9339–9347.
(58) Blake, A. J.; Brain, P. T.; McNab, H.; Miller, J.; Morrison, C. A.; Parsons, S.; Rankin, D. W. H.; Robertson, H. E.; Smart, B. A. Structure Analysis Restrained Byab {InitioCalculations}:~ The Molecular Structure of 2, 5-Dichloropyrimidine in Gaseous and Crystalline Phases. *J. Phys. Chem.* **1996**, *100* (30), 12280–12287.
(59) Mitzel, N. W.; Rankin, D. W. H. {SARACEN} -- Molecular Structures from Theory and Experiment: The Best of Both Worlds. *Dalt. Trans.* **2003**, No. 19, 3650.
(60) Zhao, Y.; Truhlar, D. G. The M06 Suite of Density Functionals for Main Group Thermochemistry, Thermochemical Kinetics, Noncovalent Interactions, Excited States, and Transition Elements: Two New Functionals and Systematic Testing of Four M06-Class Functionals and 12 Other Function. *Theor. Chem. Acc* **2007**, *120* (1–3), 215–241.

(61) Peverati, R.; Truhlar, D. G. Improving the Accuracy of Hybrid Meta-{GGA} Density Functionals by Range Separation. *J. Phys. Chem. Lett.* **2011**, *2* (21), 2810–2817.
(62) Weigend, F.; Ahlrichs, R. Balanced Basis Sets of Split Valence, Triple Zeta Valence and Quadruple Zeta Valence Quality for H to Rn: Design and Assessment of Accuracy. *Phys. Chem. Chem. Phys* **2005**, *7* (18), 3297.
(63) Weigend, F. Accurate Coulomb-Fitting Basis Sets for H to Rn. *Phys. Chem. Chem. Phys* **2006**, *8* (9), 1057.
(64) Sipachev, V. A. Calculation of Shrinkage Corrections in Harmonic Approximation. *J. Mol. Struct. THEOCHEM* **1985**, *121*, 143–151.
(65) Sipachev, V. A. Local Centrifugal Distortions Caused by Internal Motions of Molecules. *J. Mol. Struct.* **2001**, *567–568*, 67–72.
(66) Rankine, C. D.; Nunes, J. P. F.; Feixas, T. W. B. L.; Young, S.; Wann, D. A. Structure of 4-(Dimethylamino)Benzonitrile Using Gas Electron Diffraction: A New Lease of Life for the Only Gas Electron Diffractometer in the U.K. *J. Phys. Chem. A* **2018**, *122* (25), 5656–5665.
(67) Nunes, J. P. F. Personal Communication. University of York, Heslington, United Kingdom 2017.
(68) Hinchley, S. L.; Robertson, H. E.; Borisenko, K. B.; Turner, A. R.; Johnston, B. F.; Rankin, D. W. H.; Ahmadian, M.; Jones, J. N.; Cowley, A. H. The Molecular Structure of Tetra-\textit{tert}-Butyldiphosphine: An Extremely Distorted, Sterically Crowded Molecule. *Dalt. Trans.* **2004**, No. 16, 2469–2476.
(69) Wilson, A. J. C. *International Tables for Crystallography: Mathematical, Physical, and Chemical Tables*; International Union of Crystallography, 1992; Vol. 3.

Table of Contents Entry

Synopsis: Tin(II) and tin(IV) trifluoroacetates are volatile and thermally stable polymers that evaporate as discrete molecular units with entropy playing a major role in their relative volatilities. They are both suitable as precursors to CVD and potentially ALD of F-doped SnO_2.

TOC graphic: